

made, producing crystalline sphalerite films with indexes of refraction of 2.335-2.423. Deposition rates varied between 40-70 Å/min.

A Halide Transport Chemical Vapor Deposition Reactor System
for Deposition of ZnS:Mn Electroluminescent Phosphors

by

R. Todd Miller

A THESIS

submitted to

Oregon State University

in partial fulfillment of
the requirements for the
degree of

Master of Science

Completed April 7, 1995

Commencement June 1995

Master of Science thesis of R. Todd Miller presented on
April 7, 1995

APPROVED:

Redacted for Privacy

Major Professor, representing Chemical Engineering

Redacted for Privacy

Chair of Department of Chemical Engineering

Redacted for Privacy

Dean of Graduate School

I understand that my thesis will become part of the permanent collection of Oregon State University libraries. My signature below authorizes release of my thesis to any reader upon request.

Redacted for Privacy

R. Todd Miller, Author

ACKNOWLEDGMENTS

I would like to thank my advisor, Professor Milo D. Koretsky, for his guidance over the past two years.

I thank Professors Goran Jovanovic, Malcolm Daniels, and John F. Wager for serving on my committee. I also thank Dr. Wager for personal tutoring on ACTFEL device physics and insightful suggestions regarding system design.

Special thanks to Pete Myers, Chuck Meitle, Manfred Dittrich, and Art Neeley for their good advice and help.

Thanks to fellow student Jeff McKinnis for assistance, insight, and commiseration.

Thanks to Professor Art Sleight and the members of his research group, especially Pat Woodward, for x-ray diffraction measurements and interpretation.

Thanks to Wie Ming Ang for performing surface profilometry and ellipsometry measurements and for sharing his expertise in ZnS:Mn phosphors.

Thanks also to Moshe Paz and Dr. Laura King for their work in the conceptual design of the reactor system.

Finally, thanks to my wife, Anne. Without her support and encouragement this endeavor would have never come to fruition.

The financial support for this work was provided by a grant from the Advanced Research Projects Agency's Phosphor Technology Center of Excellence (Grant No. MDA972-93-1-0030).

TABLE OF CONTENTS

	<u>Page</u>
Chapter 1 - Introduction	1
Chapter 2 - Literature Review	6
2.1 Deposition Methods	6
2.2 Previous HTCVD Work	11
2.2.1 Researchers	11
2.2.2 Experimental Setup	11
2.2.3 Reaction Mechanisms	12
2.2.4 Crystallinity	16
2.3 Summary and Research Motivation	17
Chapter 3 - CVD System Design	22
3.1 General System Description and Goals	22
3.2 Hydrodynamic Considerations	25
3.3 Contamination Prevention	29
3.4 Precursor Heater Design	32
3.5 Pressure and Flow Requirements	35
Chapter 4 - Construction Details	37
4.1 Vacuum System	37
4.2 Internal Graphite Assembly	40
4.3 Precursor Heater Assembly	44
4.4 Ancillary Systems	48
4.4.1 Heat Removal	48

TABLE OF CONTENTS (Continued)

	<u>Page</u>
4.4.2 Compressed Gas Shroud	49
4.4.3 Substrate Access Hood	50
Chapter 5 - Operational Results and Design Modifications	 51
5.1 Precursor Heater Performance	 51
5.2 Flow Path Modifications	52
5.3 Film Quality	54
Chapter 6 - Conclusions and Recommendations for Future Work	 59
6.1 Conclusions	59
6.2 Recommendations for Future Work	59
Bibliography	62

LIST OF FIGURES

	<u>Page</u>
Figure 1.1 ACTFEL Panel Structure [2].	2
Figure 2.1 ZnS Transport Rates [16].	13
Figure 2.2 Competitive Adsorbtion Model [16].	15
Figure 2.3 ZnS Growth Rates [16].	16
Figure 2.4 Comparison of Crystallinities [16,19,20]. . .	18
Figure 2.5 HTCVD Luminance vs. Voltage [6].	20
Figure 2.6 Optimized HTCVD Luminance vs. Voltage [6]. .	21
Figure 3.1 HTCVD Research Reactor System	23
Figure 3.2 Reaction Chamber	26
Figure 3.3 Streamlines from Numerical Simulation [21]. .	30
Figure 3.4 Axial View of Precursor Heater	33
Figure 4.1 Vacuum System	38
Figure 4.2 Internal Assembly Schematic	41
Figure 4.3 Internal Assembly Photograph	43
Figure 4.4 Skid Assembly and Flange Carriage Photograph	45
Figure 4.5 Precursor Heater Schematic	48
Figure 5.1 Preheater Schematic	53
Figure 5.2 XRD Analysis	57
Figure 5.3 BSE Micrograph	58

LIST OF TABLES

	<u>Page</u>
Table 2.1 Comparison of ZnS:Mn Deposition Methods [18].	18
Table 5.1 Deposition Results	55

A Halide Transport Chemical Vapor Deposition Reactor System for Deposition of ZnS:Mn Electroluminescent Phosphors

Chapter 1 - Introduction

Electroluminescent (EL) displays are an exciting emerging technology in the flat panel display industry. The double insulating layer alternating current thin film electroluminescent (ACTFEL) structure was first reported by Inoguchi in 1974 using manganese doped zinc sulfide (ZnS:Mn) as the phosphor [1]. Less than a decade later, Sharp Corporation produced the first commercial product using this technology. In 1995, Planar Systems introduced the first full color display into the market.

At present, only atomic layer epitaxy (ALE) and electron beam evaporation (EBE) are used to grow ZnS:Mn phosphors in commercial production of ACTFEL displays. However, another method, halide transport chemical vapor deposition (HTCVD), shows promise to be a viable commercial method. Additionally, it is an interesting academic study, as phosphor behavior depends upon the processing parameters. To further our knowledge of this process and its films, a research scale HTCVD reactor system was built and preliminary film depositions were made. In a concurrent study within the research group, hydrodynamic behavior of the reactor is being numerically modeled.

The conventional ACTFEL display structure is depicted in

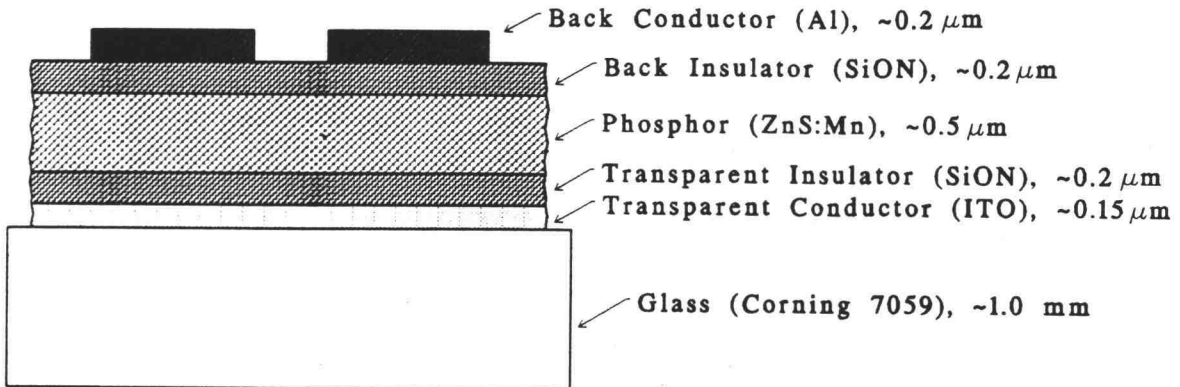


Figure 1.1 ACTFEL Panel Structure [2].

Figure 1.1 [2]. The stack consists of conductors on both sides of the ZnS:Mn phosphor layer with insulating layers separating the conductors from the phosphor. Light is generated from this structure by the following mechanism. A voltage pulse is applied across the conductors creating capacitive charges within the insulator and the phosphor layers. When the voltage exceeds a threshold voltage, the phosphor layer will shunt and electrons will accelerate through it. Along the way electrons may excite Mn dopant atoms, if the electron has sufficient kinetic energy. The electrons in the excited Mn atom can then radiatively decay, emitting a photon of visible light. ZnS:Mn emits a yellowish-orange light.

The first (front) conductor (deposited on the glass

support structure) and the first insulator must be transparent. A typical conductor material is indium tin oxide (ITO); insulating materials include silicon oxynitride (SiON), aluminum titanium oxide (ATO), and barium tantalate (BTO). The second insulating layer is also made from these oxides while the second, or "back" conductor is typically aluminum. Although the phosphor layer thickness is variable, depending upon the fabrication method, the thicknesses given in Figure 1.1 are representative [2]. The front and back conductors are deposited as straight line traces with the front traces orthogonal to the back traces. This facilitates matrix operation and the ability to perform the same functions as a cathode ray tube (CRT).

The ACTFEL display has several benefits over CRT technology. Its thin construction results in much less space and weight than a CRT. Indeed, as the viewing surface of a CRT gets larger the tube length gets longer; in an ACTFEL display the depth is nearly independent of viewing area. Typical depths of ACTFEL displays including casing are a couple of inches. Manufacture is simple and construction is rugged. ACTFEL displays also enjoy advantages over liquid crystal displays (LCDs). ACTFEL displays are emissive; consequently, they have a wide viewing angle, as opposed to the narrow viewing angle of LCDs. Also, commercial ACTFEL displays operate over a much wider range of ambient temperature than LCDs, -40 to 65°C as opposed to 10 to 40°C

[3,4]. The temperature range of operation of ACTFEL displays is limited by the electronic components, not by the EL panel. With special electronics and packaging, a much wider temperature range, -55 to 120°C, is achieved [3].

To produce a full color display, red, green, and blue light emitting phosphors are needed. Difficulties in developing a blue emitting phosphor with adequate luminance have slowed full color ACTFEL display development. Also, multicolor (red, green, yellow) ACTFEL displays consume almost twice as much power as monochrome panels (15 watts as opposed to 8 watts) [5].

Both commercial methods used to make displays require a costly and time consuming "burn in" step to overcome an initial aging phenomenon before stable EL responses are realized. At present, ACTFEL displays are used in medical, military, industrial, and transportation applications where the benefits of excellent viewing characteristics, compact size, and hardy operability outweigh the added financial cost over CRT and LCD technology.

The aging characteristics of EL devices with ALE grown phosphors are significantly different than those with EBE grown phosphors. Aging is the change with time in luminance response to an applied voltage. Recent research using an HTCVD method to grow ZnS:Mn phosphor layers has produced EL devices that exhibit the aging characteristics of either ALE or EBE phosphor devices, depending upon the processing

parameters [6]. By optimizing the HTCVD process, stable devices, those which exhibit no EL response variations with time, were produced. The development of a process capable of fabricating stable devices is obviously of great interest to ACTFEL display manufacturers. These findings are just as exciting, however, from an academic or research aspect. Since the aging mechanism is clearly related to the fabrication process, HTCVD's unique capabilities make it an excellent vehicle by which to study the relationships between process parameters and EL characteristics. An understanding of the mechanisms that occur during film deposition, and how they affect film composition, morphology, and subsequent EL characteristics, can lead to models for systematic process design. Further, understanding the relation between the physical structure of a phosphor and its EL performance can lead to better device design.

Chapter 2 overviews the various methods of depositing phosphor materials, and describes in detail previous HTCVD research and results. Comparisons between deposition methods are made. Chapter 3 describes the design of the research reactor, while Chapter 4 presents the details of the construction. Preliminary deposition data and subsequent modifications to the design are presented in Chapter 5. Conclusions and recommendations for future work are given in Chapter 6.

Chapter 2 - Literature Review

2.1 Deposition Methods

Doped ZnS ACTFEL devices have been fabricated using many different types of physical and chemical vapor deposition methods. The resulting devices exhibit varying characteristics and each process has its unique advantages and disadvantages. The physical parameters of concern include crystallinity and stoichiometry, which relate to the efficiency of the electroluminescence process, and uniformity, which relates to the practicality of manufacturing a display. To date, only electron beam evaporation (EBE) and atomic layer epitaxy (ALE) are used in commercial production of ACTFEL displays.

Physical vapor deposition (PVD) processes are based on atoms being generated from a source by a physical process, for example, through evaporation, sublimation, or momentum transfer. Atoms striking the substrate will condense, forming the desired solid thin film.

Evaporation [7,8] is the oldest of the PVD processes. It is performed at relatively high vacuum ($P = 10^{-5}$ - 10^{-7} torr) enabling collisionless transport of source vapors. Source material (ZnS and Mn) is heated resistively, inductively, or by an electron beam. The source material dissociates to form Zn and S₂ gases which recondense to form ZnS when contacting

a cooler surface. The substrate temperature during deposition is typically 125-225°C; hot enough to prevent condensation of Zn metal, yet still allow condensation of ZnS. Evaporation can deposit films very rapidly, with growth rates greater than 1000 Å per minute. The crystallinity of evaporated films, however, is not very good. Post-deposition thermal annealing at 550°C is needed to relieve stresses and improve crystallinity. Better crystallinity results in higher acceleration of electrons, and, subsequently, more light-producing scattering events.

Sputtering [9,10] relies on momentum transfer from ions in a glow discharge plasma to the source material to create precursors. Sputtering is performed at a low vacuum ($P=10^{-1}$ - 10^{-3} torr) and is capable of putting down both insulating layers as well as the phosphor without removing the substrate from the reactor. Processes that can deposit different material layers sequentially are highly desirable; handling steps and risk of contamination are lessened. At steady-state, different source atoms impinge on the substrate surface in approximately the same ratio as they exist in the target. Mass differences in the target atoms can result in preferential deposition of the heavier components, the lighter ones losing a greater percentage of their momentum to collisions with the plasma gas. Atoms that have impinged upon the substrate can also desorb; hence species which form volatile products, such as sulfur, are depleted in the film.

Also, gaseous impurities are easily incorporated into the films. Sputtered ZnS:Mn EL devices exhibit low luminescence, the result of poor crystallinity along with poor stoichiometry. Sputtering has, however, been successfully used to deposit ZnS:Tb,F EL films. High kinetic energy Tb atoms force their way into the crystal structure, overcoming the ionic radius and valence mismatches.

Multi-source deposition (MSD) [11] is a modified evaporation process where the film composition is controlled through component vapor pressures rather than source composition. Sources of components (Zn, S, and Mn) are individually heated allowing control and manipulation of vapor pressures and, subsequently, gas and film compositions. This process requires very precise temperature control. MSD has produced highly crystalline films with good stoichiometry. Very large crystallites (100-200 nm) in the hexagonal (wurtzite) structure have been produced. The only apparent drawback to MSD is that, like all PVD processes, multipanel processing is hampered by the line-of-sight positioning necessary for source to substrate transport.

Chemical vapor deposition (CVD) differs from PVD in that the film precursors are generated via chemical reactions as opposed to physical means. While PVD is performed in the molecular flow regime to minimize gas collisions, CVD is performed in the viscous regime to promote interactions that lead to chemical reactions. There are "gray areas" where a

process could be considered either CVD or PVD; evaporation of compounds, for example. Heated ZnS dissociates to Zn and S₂ gases, not ZnS_(g). This reaction occurs in both evaporation and, as will be shown, halide transport CVD (HTCVD).

Atomic layer epitaxy (ALE) [12,13] is the only CVD process by which ACTFEL displays have been commercially produced. ZnS deposition occurs by alternately feeding gaseous precursors such as ZnCl₂ and H₂S into the reaction chamber with an intermittent inert gas purge. The Mn dopant is introduced as MnCl₂ in lieu of ZnCl₂. The substrate temperature (500°C) provides a surface energy in between the stronger Zn-S bonds and the weaker Zn-Zn and S-S bonds. Thus, only the former are stable throughout the inert gas purge; correspondingly deposition occurs one monolayer at a time resulting in excellent stoichiometry and crystallinity. Crystallite sizes are 2-3 times larger than other methods, except MSD. Additionally, like sputtering, ALE can be used to deposit insulator, phosphor, and insulator sequentially. The disadvantages of ALE are slow deposition rates (10-50 Å/min) and undesirable aging phenomenon in EL response.

Recent phosphor deposition research has focused on metalorganic CVD (MOCVD) [14,15]. The impetus is that MOCVD growth temperatures can be lower than other CVD methods (300°C as opposed to 500°C), resulting in less diffusion in and between films layers. MOCVD also potentially exhibits excellent crystallinity. A typical MOCVD setup bubbles H₂

through liquid metalorganic precursor solutions to carry them into the deposition chamber. Dimethyl-zinc (DMZ) or diethyl-zinc (DEZ), and tricarbonylmethyl-cyclopentadienyl-manganese (TCM) have successfully been used as Zn and Mn precursors. Sulfur is introduced as H_2S or diethylsulfide (DES). These metalorganics decompose on the heated substrate surface to form the ZnS:Mn film. Experimental processes have been conducted in the mass transfer controlled regime, consequently the hydrodynamics of the system must be carefully designed to ensure film uniformity. Film stoichiometry is easily controlled through relative carrier gas flow rates and precursor liquid temperatures. The crystal structure depends mainly upon growth temperature; lower temperatures (300-400°C) result in a zinc blende structure, higher temperatures (400-500°C) in a wurtzite.

In the halide transport CVD (HTCVD) [6,16,17] process, a carrier gas of argon (Ar) or hydrogen (H_2) is passed over a solid precursor of ZnS. The ZnS is heated to 900-1000°C to generate a sufficient vapor pressure for deposition. Solid ZnS dissociates to Zn and S_2 gases which are carried to the reaction chamber where adsorption and reaction to ZnS can occur on the substrate surface. The Mn dopant is transported to the reaction chamber by a carrier gas of HCl. Solid Mn, heated to 700°C, reacts with the HCl to form gaseous precursors of $MnCl_2$ and H_2 . Films produced by HTCVD have good stoichiometry and crystallinity in the wurtzite structure.

HTCVD's hot-wall, diffusion furnace setup is quite amenable to commercial scale production. Additionally, ZnS:Mn films can be grown which show no deleterious aging effects.

2.2 Previous HTCVD Work

2.2.1 Researchers

From 1991 to 1992 Akiyoshi Mikami et al. of Sharp Corporation's Central Research Laboratories in Japan published three papers on doped ZnS EL devices they produced using HTCVD [6,16,17]. Their work showed the HTCVD process capable of producing ACTFEL devices that exhibited luminance characteristics similar to those of either ALE or evaporated devices, depending on the process parameters. By setting the temperature at the deposition mode transition and optimizing the other process parameters, they were able to produce a device that exhibited no change in luminance with time, i.e., a stable device. This is the only published work on HTCVD of doped ZnS phosphors.

2.2.2 Experimental Setup

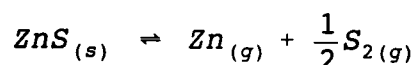
The HTCVD system [16] was comprised of a vacuum system, a quartz processing tube heated by a resistive furnace, and internal quartz tubes, each independently heated, in which solid phase precursor chemicals were placed. ZnS powder and solid Mn placed in the tubes were heated to temperatures of

900-1000°C and 700°C, respectively. The ZnS dissociated to Zn and S₂ gases which were carried to the reaction chamber by a flow of either Ar or H₂. The Mn reacted with a gas stream of HCl to form MnCl₂ and H₂. The ZnS carrier gas flow rate was kept constant at 100 standard cubic centimeters per minute (sccm), while the HCl flow rate was varied from 0 to 5 sccm. The dopant concentration in the deposited film was controlled by varying the HCl flow rate. The substrate temperature was varied between 300 and 600°C, while total gas pressure was maintained at less than 1 torr.

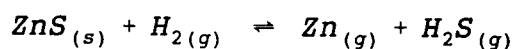
2.2.3 Reaction Mechanisms

The HTCVD method of producing ZnS:Mn films consists of three separate reactions: the dissociation of solid ZnS to gas-phase Zn and S₂, the reaction of HCl gas with solid Mn to form MnCl₂ and H₂ gases, and the deposition of these species at the substrate surface to form the solid film.

When H₂ is used as the ZnS carrier gas, it is possible that the sulfur is transported as H₂S as well as S₂. The corresponding reaction equations are:



and



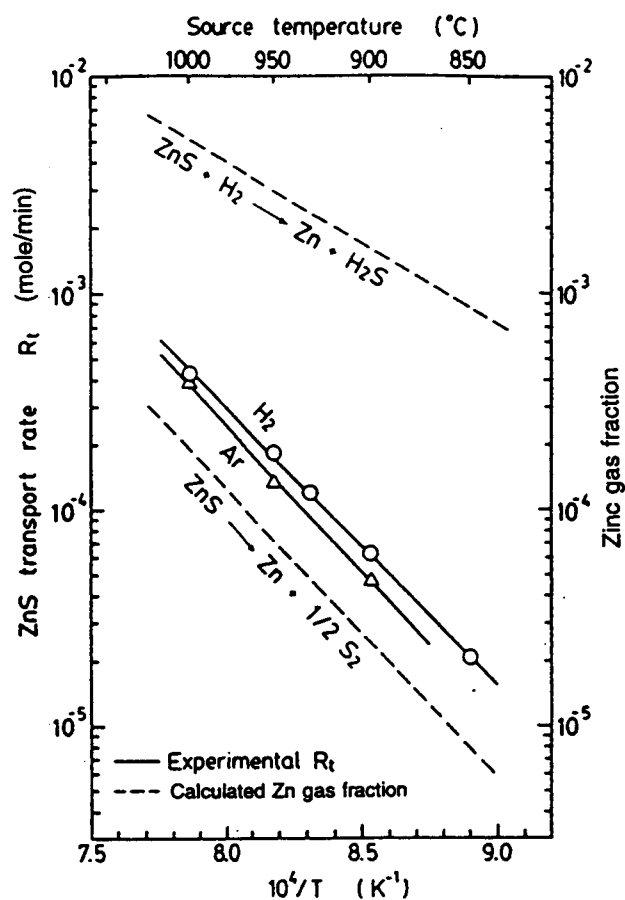


Figure 2.1 ZnS Transport Rates [16].

Figure 2.1 shows the temperature dependencies of ZnS transport using Ar and H_2 as carrier gases in an Arrhenius type plot. Also shown are theoretically calculated Zn gas fractions for both reaction equations. The data show ZnS transport to be a highly activated process. The similar slopes, and therefore activation energies, of the transport temperature dependencies indicate the same reaction mechanism for both. The fact that these slopes coincide with the temperature dependencies of the Zn gas fractions calculated from the first reaction indicates that H_2 does not chemically

participate in the transport of ZnS.

Transport rates were determined by weighing the solid precursor charge before and after deposition. Species gas fractions were calculated using the relations:

$$K = P_{Zn} P_{S_2}^{\frac{1}{2}}$$

and

$$K = \frac{P_{Zn} P_{H_2S}}{P_{H_2}}$$

where K is the equilibrium constant and p is the species partial pressure. K is a function of temperature only; values can be calculated from tabulated thermodynamic data. The gas species fractions are the ratio of their partial pressures to total system pressure. The gas species calculation also requires knowledge pertaining to crucible volume and carrier gas flow rates.

The solid Mn precursor reacts with the HCl carrier gas by the reaction:



Mn transport, therefore, is strongly related to HCl flow rate. It has been shown that doping concentrations can easily and accurately be controlled by modulating the HCl flow. To obtain doping concentrations in the range of 0.5 at%, HCl to

ZnS carrier gas flow ratios are $\sim 1/100$ [16].

A competitive adsorption model was proposed as the mechanism by which Mn is incorporated into the ZnS film. A conceptual schematic of the mechanism is shown in Figure 2.2 [16].

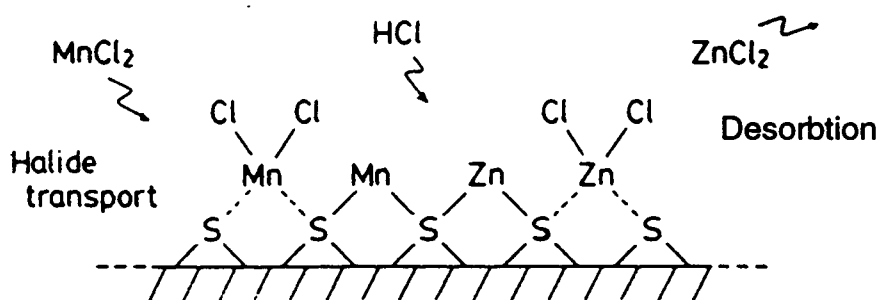


Figure 2.2 Competitive Adsorption Model [16].

Manganese dichloride chemisorbed to the S surface releases its Cl atoms which in turn react with a loosely bonded Zn atom. Zinc dichloride, whose vapor pressure is higher than that of MnCl₂, is formed and desorbs from the surface. The Cl atoms, in effect, etch Zn from the surface, leaving an open site for adsorption of Zn or MnCl₂.

Film growth rates are clearly reaction-rate controlled at temperatures up to 500°C, as seen in Figure 2.3 [16]. The growth rate goes through a transition, then drops precipitously as temperatures are increased above 600°C, indicating a change in the mode of deposition. Gas-phase

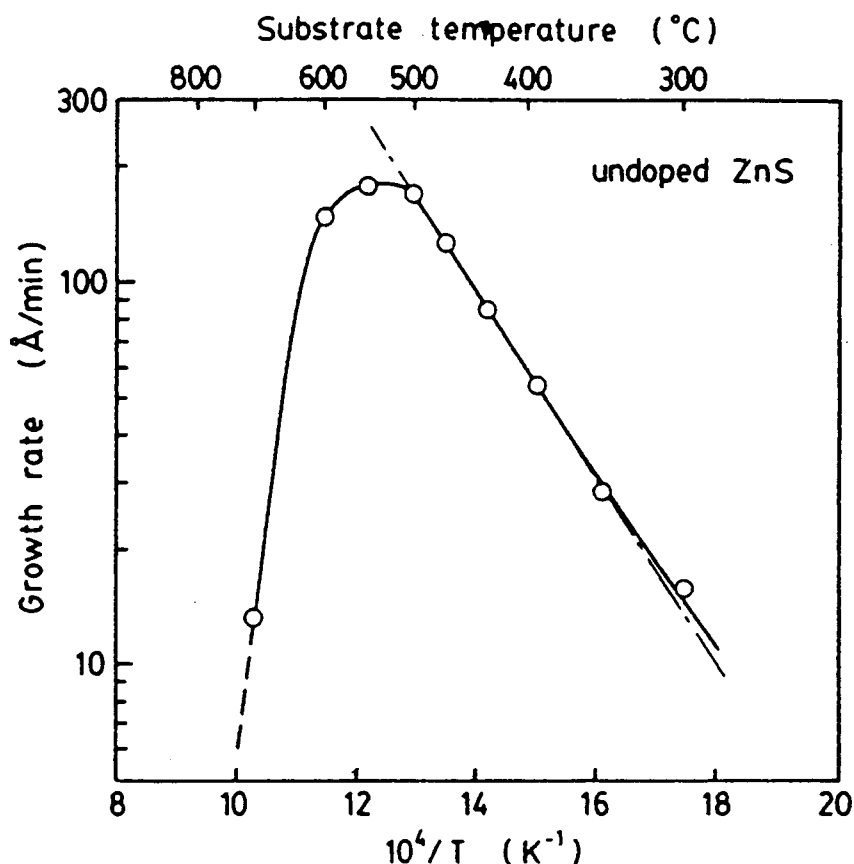


Figure 2.3 ZnS Growth Rates [16].

nucleation, desorption, and mass transfer are some of the phenomenon that may account for these changes; more investigation is needed.

2.2.4 Crystallinity

The phase transition between the sphalerite and wurtzite forms of ZnS occurs at 1020°C. It is therefore expected that ZnS thin films form the sphalerite or cubic crystal structure at deposition temperatures between 400-600°C. However, the addition of the Mn dopant in concentrations of 0.05 to 4

atomic percent under the same growth conditions causes the film to change to the wurtzite or hexagonal structure [16]. Moreover, the crystallinity and morphology are improved and produce better electroluminescent characteristics. At higher Mn concentrations, a MnS rock salt phase in a hexagonal ZnMnS solid solution appear, accompanied by a degradation of electroluminescence.

At constant doping concentrations, the crystal structure and quality varies with temperature. Doped at 0.4 at% Mn the crystallinity of a ZnS film is polycrystalline at 450°C, but changes to a single crystal hexagonal structure at 500°C [16].

2.3 Summary and Research Motivation

The characteristics and conditions for the deposition methods discussed in section 2.1 are shown for comparison in Table 2.1 [18]. EBE's high deposition rates make it attractive from a production throughput standpoint, as does its low deposition temperatures. The high luminous efficiencies in panels produced by HTCVD and MOCVD make for better product performance.

Figure 2.4 shows the degree of crystallinity for some of the methods [16,19,20]. Sputtered films, which have very poor crystallinity, and MSD films, which have exceptional crystallinity, are not shown. Of those methods shown, ALE produces films with the best crystallinity; its crystallite

Table 2.1 Comparison of ZnS:Mn Deposition Methods [18].

Conditions and characteristics	PVD			CVD		
	Sputtering	EBE	MSD	MOCVD	HTCVD	ALE
Deposition rate (Å/min)	>100	>1000	~300	>100	>100	10-50
Substrate temperature (°C)	200	200	300	300-500	500	500
Crystal Structure	zb	zb	zb,w	zb,w	w	w
Luminance (cd/m ²)	>1500	>3000	>3000	>3000	>3000	>3000
Luminous efficiency (lm/W)	~2	~3	~3	>4	>4	~3

luminance measurements at 1 kHz; zb = zinc blende, w = wurtzite

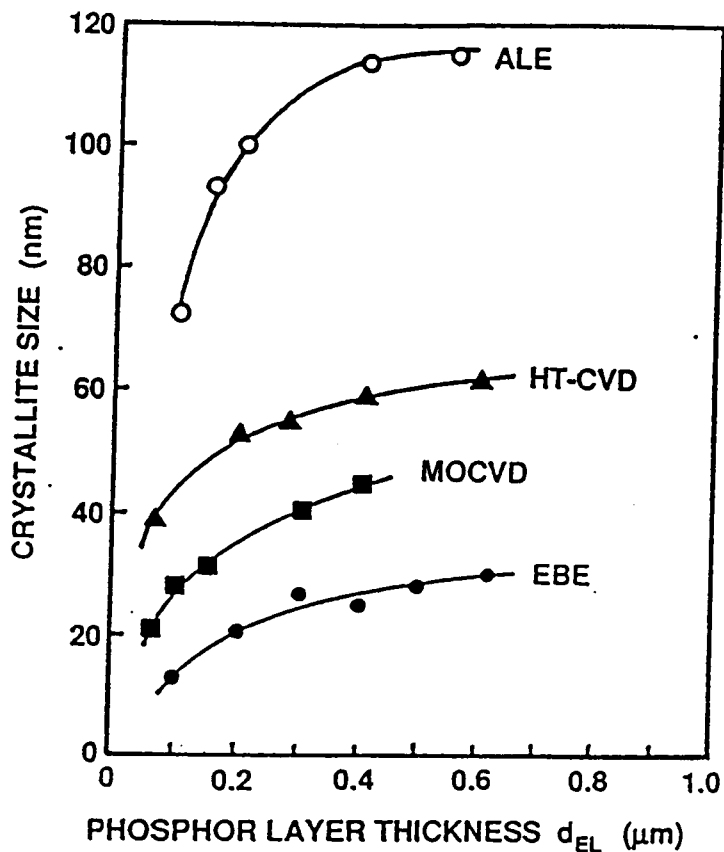


Figure 2.4 Comparison of Crystallinities [16,19,20].

sizes are twice those of the next best method. Again, EL characteristics are believed to improve with crystallinity.

These data show that HTCVD compares favorably to the other deposition methods. HTCVD deposition rates are lower than EBE's, but higher than ALE's. HTCVD produces films of lesser crystalline quality than ALE, but better than EBE. Luminance is about the same in all, but HTCVD and MOCVD have higher luminance efficiencies. MOCVD has characteristics similar to those of HTCVD; however, MOCVD experiments were performed using cold-wall, mass transfer-controlled reactors. Cold-wall CVD systems are not as amenable to multipanel processing as hot-wall, diffusion systems such as HTCVD and ALE because the hydrodynamics must be more carefully controlled to obtain product uniformity. PVD methods, including MSD, require line-of-sight placement of substrates to source materials; multipanel processing is therefore hindered by the basic principle behind these methods.

What makes HTCVD really unique is that the fundamental nature of EL response varies with processing parameters, especially substrate temperature. Figure 2.5.a [6] shows the luminance-voltage (L-V) curves for a phosphor deposited using HTCVD at a substrate temperature of 450°C. The L-V curve "rigidly" shifts during the first 100 hours of operation, requiring higher and higher voltages to generate luminance. This is the same behavior exhibited by EBE devices. Figure 2.5.b [6] is the L-V curves for an HTCVD device deposited at

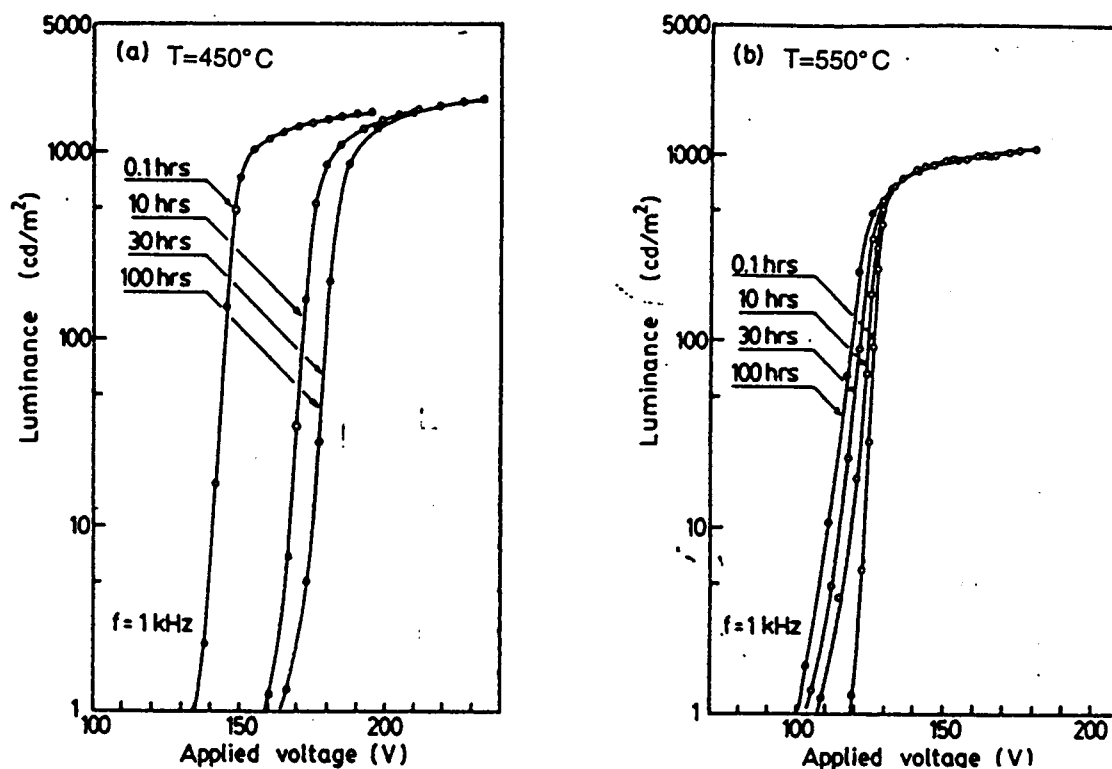


Figure 2.5 HTCVD Luminance vs. Voltage [6].

a substrate temperature of 550°C . The peak voltage required remains the same, but the threshold voltage decreases, "softening" the slope of the curve. This response is also displayed by ALE devices. By controlling the substrate temperature at 500°C and optimizing the other parameters (system pressure of 0.1 torr, phosphor thickness of $0.7\ \mu\text{m}$, Mn concentration of 0.3 at%), the HTCVD process has been proven capable of producing stable devices [6]. L-V curves for these are shown in Figure 2.6 [6].

EL films with no aging response occur at precisely the point where the growth mechanism changes from being kinetically limited to something else. Therefore, it makes

sense to examine aging phenomenon through an exploration of process parameters and their relation to device performance.

To summarize, HTCVD holds commercial promise as a high throughput process capable of producing stable devices. Its unique EL response variations also make it a worthy academic study, possibly being a means of elucidating the precise relations between material compositions and EL response.

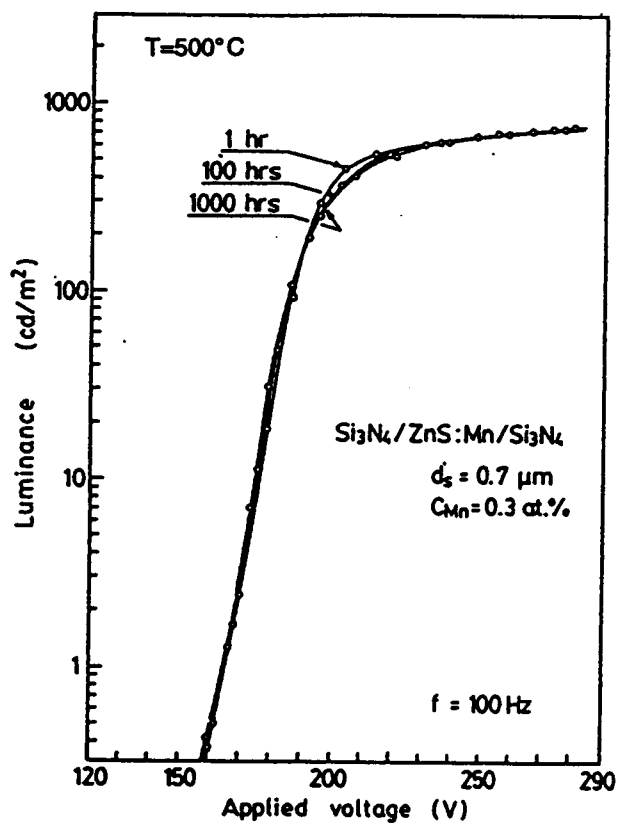


Figure 2.6 Optimized HTCVD Luminance vs. Voltage [6].

Chapter 3 - CVD System Design

3.1 General System Description and Goals

It was desired to build a high purity research reactor that was versatile in operation so that important process parameters, including physical configuration, could be easily manipulated. To this end, a modular type design with a reaction chamber made of a machinable ceramic inside a stainless steel shell was pursued. The major elements of the research reactor are depicted in Figure 3.1.

A stainless steel shell (process tube) functions as the pressure barrier, letting the ceramic reaction chamber control the hydrodynamics and provide a barrier to contamination from the stainless steel. Boron nitride was the first choice of material for the reaction chamber, however its use was cost prohibitive for a first version of the design. High purity graphite, as used in ALE systems, was chosen instead.

The process tube is placed in a three-zone resistive furnace to generate uniform deposition temperatures of 450-600°C. The hot-wall design is typical of CVD (diffusion) systems.

Gas-phase reactants are generated by heating solid reactant precursors to induce dissociation or reaction with carrier gases. Zinc sulfide dissociates to Zn and S₂, while Mn reacts with HCl to form H₂ and MnCl₂. Zinc sulfide must be

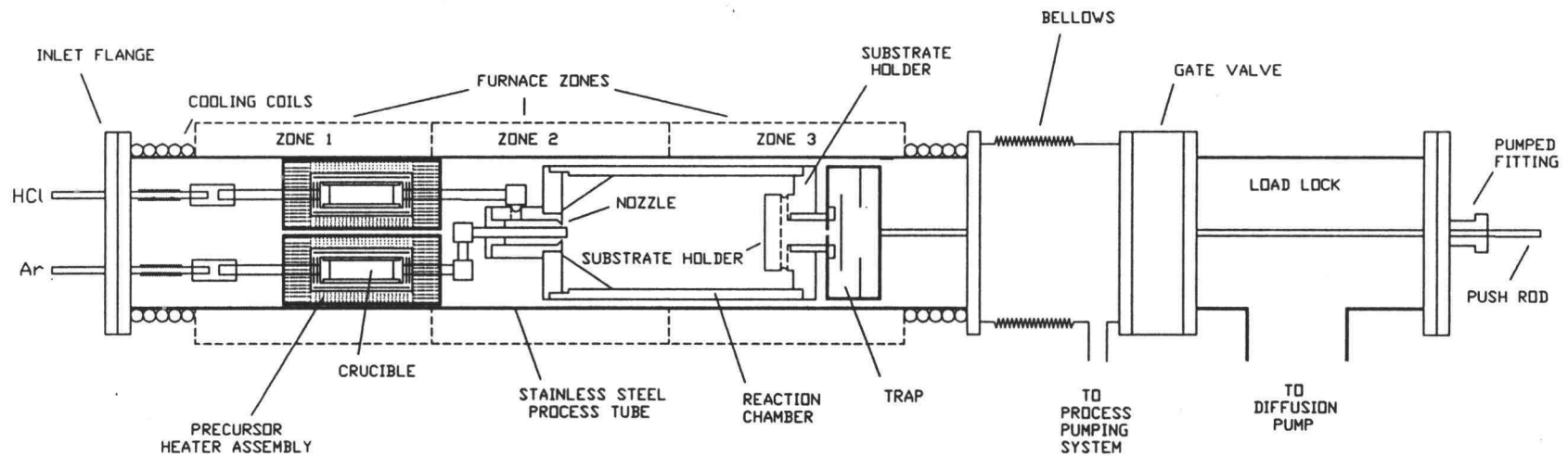


Figure 3.1 HTCVD Research Reactor System.

heated to a temperature higher than 900°C, and Mn higher than 700°C, before significant precursor fluxes are realized. To achieve these high temperatures, insulated heaters were built around each solid precursor crucible. Additionally, it was desired to minimize gas-phase nucleation during transport and reactant loss to deposition on the delivery tube surfaces. Consequently, the heated crucibles were placed internal to the furnace in close proximity to the reaction chamber. The internal heaters, then, had to be capable of supplying sufficient power to achieve their respective temperatures above the uniform furnace temperature; the temperature difference, ΔT , required of the ZnS heater is 300-550°C, and of the Mn heater is 100-250°C.

Carrier gases are used to transport gaseous precursors from the crucibles to the reaction chamber. Argon was chosen as the ZnS carrier gas because its inertness simplifies the chemistry. A stream of HCl reacts with the solid Mn, creating $MnCl_2$ and H_2 gaseous precursors. The gas flows enter the reaction chamber through a coaxial nozzle. The nozzle induces prescribed mixing to ensure uniform gas composition when the flow reaches the substrate at the other end of the reaction chamber. Residual gases exit through ports bored into the substrate holder. A mesh trap catches unreacted metals before exhausting to the vacuum system.

The system was designed with a load-lock chamber for ease of changing substrates. The substrate holder is moved back

and forth from the load-lock to the reaction chamber by a push rod. The load-lock allows the process tube to remain under vacuum; thus, only the substrate holder in the load-lock chamber requires outgassing with every substrate change.

The overall size of the reactor system was designed around a 2 inch square substrate size. Glass substrates are provided by Planar Systems with the transparent ITO electrode already sputtered on. In order to accommodate perpendicular flow and adequate room for the internal assembly, a 6 inch ID furnace was procured. Correspondingly, the process tube has a 6 inch OD.

A 100 l/s Roots blower with backing pump is used as the vacuum system. For the total design flow of 120 sccm at 1 torr, the blower system is quite adequate for a system with reasonable conductance.

3.2 Hydrodynamic Considerations

In designing the research reactor special attention was paid towards minimizing gas-phase nucleation. Particle formation in the gas phase, and subsequent incorporation into a film, can result in degradation of EL performance. To this end, the reactor was designed to induce mixing of species for uniformity of deposition, yet still maintain an overall plug-type flow.

As shown in Figure 3.2, the reaction chamber has a

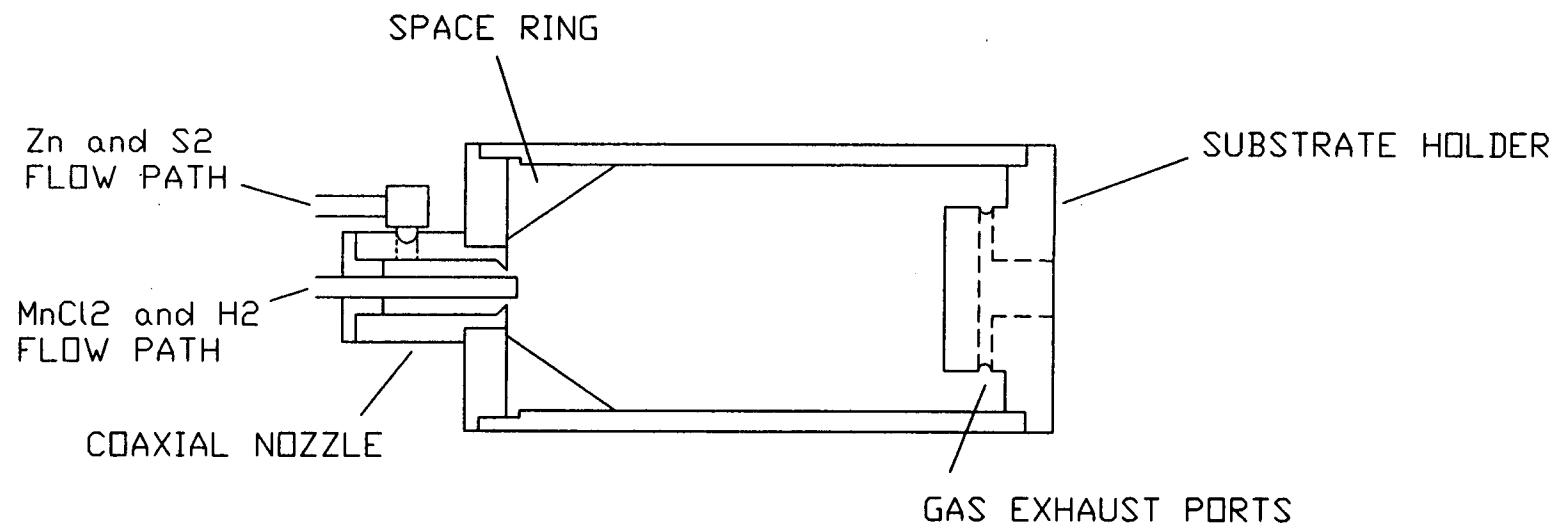


Figure 3.2 Reaction Chamber.

coaxial nozzle assembly and an internal shape designed to minimize dead space and recirculation cells. Zn and S₂ gas from the solid ZnS precursor flows through the annulus of the nozzle at a flow rate two orders of magnitude greater than that of MnCl₂ and H₂ gas flowing through the center tube. The angled lip of the nozzle forces the two gas streams to mix as they flow towards the substrate. By controlling the mixing and flow, gas-phase nucleation can be minimized.

Substrates may be positioned either parallel or normal to the gas flow. In a normal flow configuration, the substrate is placed directly onto the substrate holder. For parallel flow, a blade is mounted into the holder, with the substrates placed on either or both sides of the blade. The modularity of the assembly will also accommodate other configurations.

Gas flow exits the reaction chamber via small ports bored radially into the substrate holder that connect with a larger hole bored axially. The ports are evenly spaced to promote axisymmetric flow around the substrate holder.

Boundary layer formation is another hydrodynamic consideration when operation is in the viscous flow regime, as in CVD systems. Gaseous species must diffuse through the boundary layer before surface reactions can occur; if this diffusion is the rate-limiting step, uneven boundary layer thickness will result in uneven deposition. Therefore, in mass-transfer controlled systems, the flow geometry must be carefully designed.

For the parallel flow configuration, boundary layer formation can be approximated by the following equation for parallel flow along a flat plate

$$\delta \propto \sqrt{\frac{\nu x}{u_{\infty}}}$$

where δ is the boundary layer thickness, ν is the fluid viscosity, x is the distance along the plate, and u_{∞} is the bulk fluid velocity. For a constant bulk velocity and viscosity, the boundary layer thickness increases as the square root of the axial distance along the substrate holder blade.

However, the bulk velocity can be increased by reducing the area of the flow channel. Designing a channel reduction that is proportional to the axial distance down the blade can result in a uniform boundary layer and improved deposition uniformity. To effect a uniform boundary layer in the research reactor for a flow of 100 sccm, the channel area will need to decrease as described by the function

$$A = \frac{230}{x}$$

where A is the channel area in cm^2 and x is the axial distance down the substrate blade in cm. Due to edge effects, the equation is only valid for positions further than 2 cm along the substrate holder. A few different configurations can be

substrate placed normal to the gas flow. This affords the simplest configuration for the concurrent numerical modeling effort. Due to symmetry, only half the reaction chamber needs to be modeled. Simulation results can be used to evaluate future design modifications and for data analysis. Figure 3.3 shows streamlines for 100 sccm flow through the reaction chamber at a uniform temperature of 500°C and a pressure of 1 torr [21]. In normal flow there is a stagnation point at the center of the substrate; this can be used to gain information about the process mode changes discussed in section 2.2.2. In the reaction controlled regime, uniform deposition should result. If mass transfer controlled, however, the hydrodynamics should create axisymmetric nonuniformities in the film.

3.3 Contamination Prevention

Zinc sulfide is the matrix material into which the light emitting component is doped. Dopant materials are chosen based on their ability to absorb the kinetic energy of electrons moving in the electric field through the phosphor, and to radiatively emit the energy as light. The

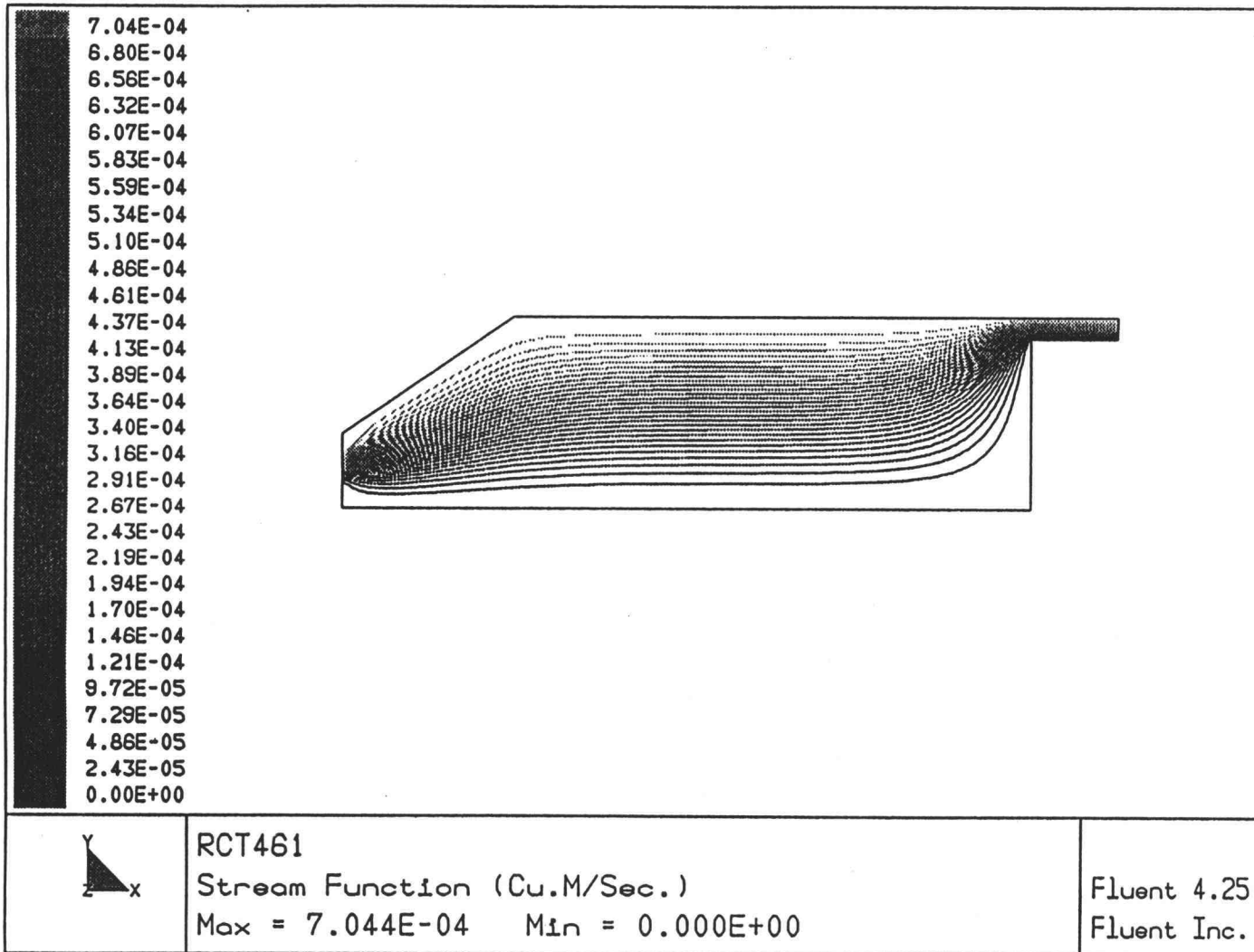


Figure 3.3 Streamlines from Numerical Simulation [21].

characteristics of such a dopant are deep energy levels, large cross sections for impact excitation, and stability in high electric-field environments. Manganese (yellow), terbium (green), samarium (red), europium (red), cerium (blue-green), and promethium (white) have been used as dopant materials [22]. Other materials such as the nickel (Ni), chromium (Cr), and iron (Fe) in stainless steel lose energy to processes other than light emission. Contamination with these metals degrades the electroluminescence of a device. Since the dopant levels are on the order of 1 atomic percent, even trace amounts of contamination from the stainless steel could effect the performance of the resulting phosphor. To minimize this contamination, the high temperature chemistry is confined inside a boundary of inert ceramic. The use of stainless steel must be limited to regions of low temperature where the vapor pressures of the stainless steel components are insignificant, i.e., the room temperature delivery lines and the extreme end of the process tube. Welded stainless steel glands are necessary to provide a vacuum-tight feed through the flange. A short bellows allows for thermal expansion and easier assembly. A compression fitting provides the transition from stainless steel to graphite.

3.4 Precursor Heater Design

To reduce long residence times and unprescribed mixing that can lead to gas-phase nucleation, the distance between the precursor heaters and the reaction chamber should be minimized. Since the precursors are to be heated above the deposition temperatures, the heaters may be placed inside the process tube. The power provided by these heaters need only be enough to generate the ΔT the precursor is above the furnace temperature.

The goal of the precursor heater design was to minimize heat loss and subsequent power requirements while working within the spacial restrictions of the process tube. To gain closest proximity to the reaction chamber the heaters must be placed side by side. Therefore, the maximum outside diameter of a heater is 2.875 inches. An axial view of the heater design concept is shown in Figure 3.4. A stainless steel tube is used as an outer shell to mechanically support the insulation and radiation shields inside. The graphite crucible is heated by resistive wire wrapped around it. The outside diameter of the crucible and element construction is 1.5 inches.

The two main paths of heat loss are radially, where the insulation layer is the thinnest, and axially through the thermally conductive graphite tubing. Axial heat losses through insulation are assumed to be negligible as are

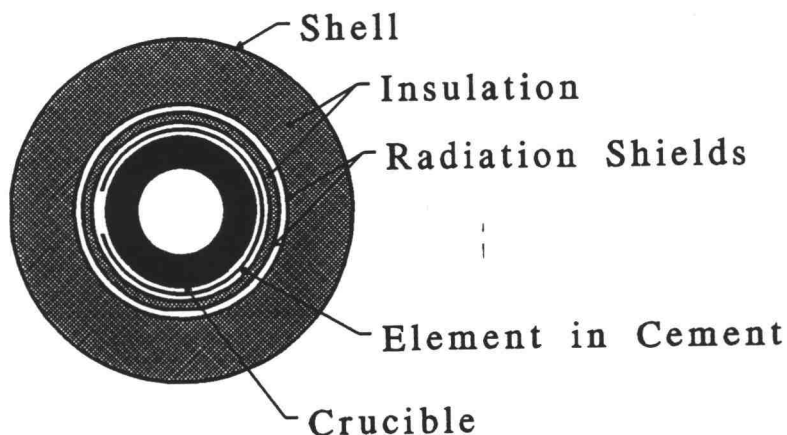


Figure 3.4 Axial View of Internal Heater.

sublimation energies and convective losses to carrier gases.

The radial heat loss was calculated using a simplified conduction model. The entire annulus between the crucible and shell was assumed to be filled with insulating zirconia felt (thermal conductivity, $k=0.003$ W/in \cdot° K). This is a conservative model since at 975° C thermal radiation is a significant mode of heat transfer, which shielding should effectively inhibit. However, the ability of the metal foils to retain their emissive and absorptive properties in the potentially corrosive environment was questioned, therefore the heater was modeled without them.

The steady-state conductive heat transfer in the heater assembly is described by Fourier's law, written as

$$q_r = -kA \frac{dT}{dr} = -k(2\pi rL) \frac{dT}{dr}$$

where q_r is the radial heat flux, k is the thermal conductivity of the zirconia felt, r is the radial distance from the center of the crucible, and l is the crucible length (3 inches). Using the boundary conditions of 975°C at the outer edge of the crucible and element construction ($r=0.75$ inches), and 500°C at the inside of the shell ($r=1.44$ inches), the radial heat loss is calculated to be 41 watts.

Steady-state heat loss through the graphite tubes is also calculated using Fourier's law,

$$q_x = -kA \frac{dT}{dx}$$

where q_x is the axial heat flux and A is the cross sectional area of the graphite tube (0.12 in²). Using boundary conditions of 975°C at the crucible ends and 500°C 3 inches down each tube, the combined heat loss is 97 watts. The total steady-state heat load is therefore about 140 watts.

Additional power was desired to reduce the heat-up times and as a contingency so that steady-state operation is well within the performance capability of the heater. Thus, as an initial design specification, an internal heater should be able to generate ~200 watts of resistive heat. Performance data can be used in modifying the design, if necessary.

3.5 Pressure and Flow Requirements

System pressure in the reaction chamber was desired to be 1 torr or less. A 100 l/s Roots blower and mechanical backing pump set were available for use. With the total flow anticipated to be around 120 sccm, or 1.5 l/s at 1 torr, this pump set should be quite adequate for a system with reasonable conductance.

The blower is connected to the process tube via 6 ft of 1.5 inch tubing. Also in this line is a molecular sieve trap and three 90° elbows. The conductance of the sieve trap is 12 l/s while the elbows have a conductance equivalent to 1 ft of tubing; the 7 ft of equivalent tubing has a conductance of 3.1 l/s. The only other restriction that needs to be considered is the exhaust ports through the substrate holder. The six, 1/4 inch diameter parallel ports have a combined conductance of 7.4 l/s. The total conductance is, therefore, 1.8 l/s, adequate for the intended use.

A diffusion pump was incorporated into the system for use in outgassing the system. However, to date it has not been used in processing applications.

Mass flow controllers are used to accurately deliver carrier gases to the system. Allowances were made for an inert purge gas flow through the annulus between the graphite assembly and the stainless steel shell. The gas lines were

also configured so the HCl lines could be purged after use to minimize corrosion to the line, regulator and mass flow controller.

Chapter 4 - Construction Details

4.1 Vacuum System

As mentioned previously, the stainless steel process tube provides the pressure barrier to maintain the vacuum. Stainless steel allows use of copper gasket flanges, which can be used to higher temperatures than o-ring seals that are limited to 150°C. Metal gasket glands were chosen over o-ring face sealing glands for the same reason. Tungsten inert gas (TIG) welding was used to make all steel welds. This method reduces the formation of oxides during the welding process; oxides can be a source of impurities during deposition. Additionally, all welds were either made from the vacuum side or through welded from the atmospheric side to avoid creation of gaps or void spaces that could harbor contaminants.

The vacuum system consists of a Stokes model 148 MBVX combination Roots blower and mechanical backing pump for exhausting process gases during deposition, and a 6 inch NCR diffusion pump with Welch model 1397 backing pump for outgassing. System pressure (50 mtorr to 2 torr) is measured by a capacitance manometer positioned on the inlet flange. Pressure is controlled by varying the blower motor speed and/or Ar flow in the annulus between the shell and internal assembly. Thermocouple gauges positioned in the rough and process lines facilitate valving operations.

A schematic of the vacuum system is shown in Figure 4.1.

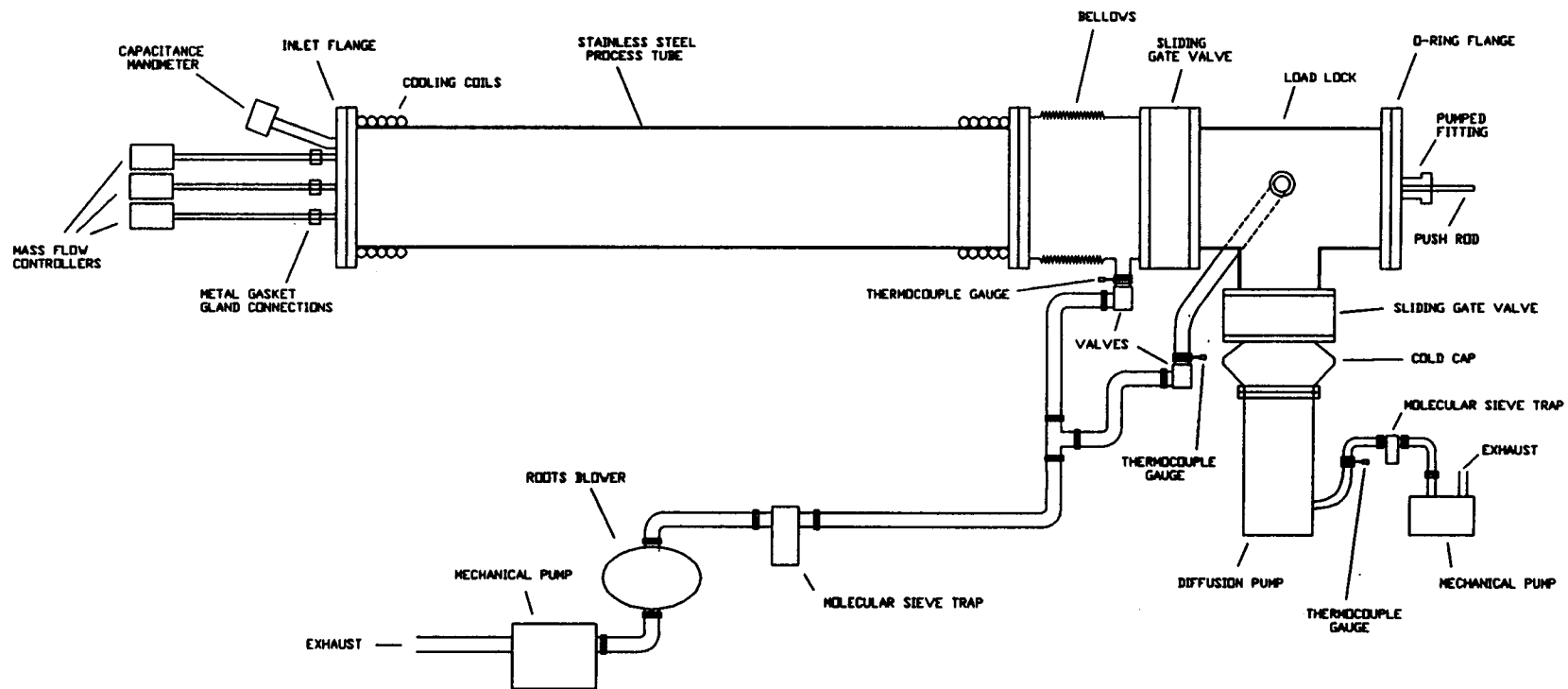


Figure 4.1 Vacuum System.

Mass flow controllers are connected to glands on the inlet flange by 1/4 inch stainless steel tubing. There are three glands; one each for the ZnS carrier gas, the Mn carrier gas, and for a purge through the annulus between the shell and the internal assembly. The inlet flange and the connecting flange on the other end of the shell are 8 inch copper gasket flanges. Since the process tube is inside the furnace sitting on one table and the load-lock is mounted onto the diffusion pump hanging from another, a bellows spoolpiece is needed to connect the two. A 2.75 inch copper gasket stub off the bellows spoolpiece connects it to the process line to the blower. A sliding gate valve isolates the process tube from the load-lock while changing substrates. A 2.75 inch copper gasket stub off the load-lock connects it to the rough line to the blower. On the end of the load-lock where high temperatures are not a problem, an o-ring seal flange is used for easy access. Two quartz viewports allow visibility for alignment of the substrate holder to the reaction chamber. The substrate holder push rod moves through an o-ring and Teflon sealed, pumped fitting. A sliding gate valve isolates the diffusion pump from the load-lock. A cold cap is used to prevent backstreaming of diffusion pump oil into the load-lock, while a molecular sieve trap is used to catch mechanical pump oil backstreaming in the process line.

4.2 Internal Graphite Assembly

The contamination-barrier-inside-a-pressure-barrier design creates some interesting mechanical challenges, as precursor access and substrate exchange now become more complicated.

It was desired to have a means of changing substrates without having to break vacuum in the process tube. To this end, the substrate holder was designed as a "plug" to the back end of the reaction chamber. A push rod connected to it allows movement between the load-lock and the reaction chamber.

To replenish the solid precursors, the crucibles must be removed from the process tube. The easiest way to do this is to remove everything in the flow path from the reaction chamber back to the inlet flange. The graphite tubing and connections are fragile; consequently, a support structure was built to hold everything in position.

A schematic of the entire internal assembly and substrate holder is shown in Figure 4.2. After entering the process tube through metal gasket glands welded to the inlet flange, carrier gases pass through a short 1/4 inch diameter stainless steel bellows to allow for differences in thermal expansion between the graphite components and the stainless steel support rods. The flow path material changes from stainless steel to graphite before entering the high temperature regions

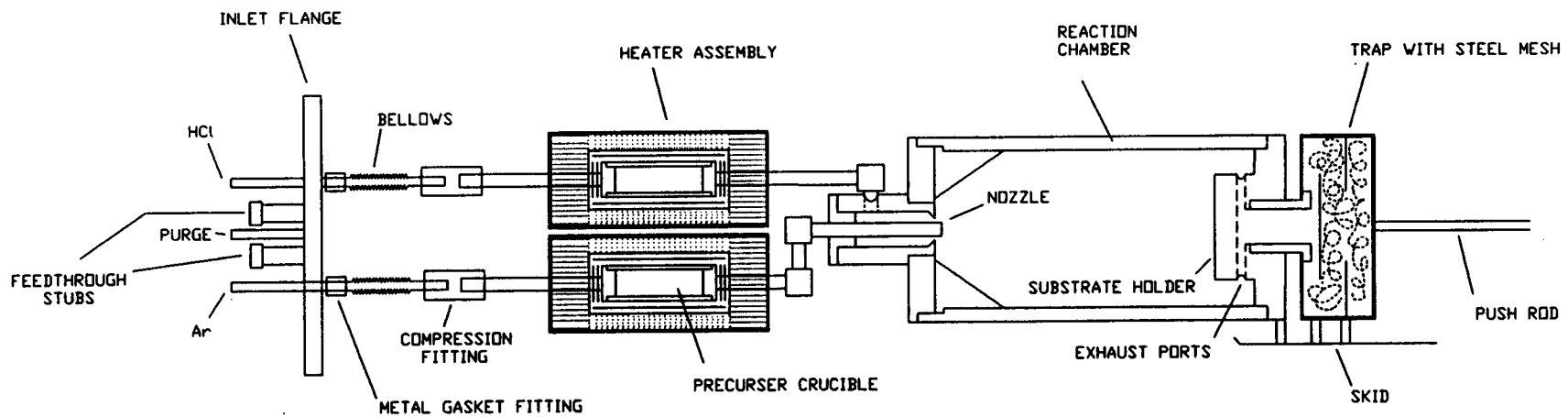


Figure 4.2 Internal Assembly Schematic.

using an o-ring compression fitting. The temperature, however, is already too high for elastomeric o-rings, so a graphite cement is used instead. The 3/16 inch ID graphite tubing leads to and from precursor crucibles, using 90° elbows to gain proper alignment to the nozzle. The coaxial nozzle allows prescribed mixing of gaseous precursors. Premature or uncontrolled mixing can lead to gas-phase nucleation and subsequent particle formation. The reaction chamber has angled rings to eliminate dead spaces and recirculation cells. Overall flow through the reaction chamber should be as plug-like as possible. The longer the residence time, the greater the likelihood of gas-phase nucleation. Gases leave the reaction chamber via six 1/4 inch diameter holes bored radially in the substrate holder. The holes are evenly positioned to promote axisymmetric flow through the reaction chamber. These holes connect to a 1 inch axial path to a trap filled with stainless steel mesh. The mesh provides a large surface area for capture of undeposited materials.

The internal assembly is attached to and supported by 3/16 inch diameter stainless steel rods screwed into the inlet flange. A removable wheeled support attached to the inlet flange allows easy withdrawal of the internal assembly onto a removable work table. The internal assembly, positioned on the work table, is pictured in Figure 4.3.

The substrate holder and trap are mounted onto an adjustable skid assembly to facilitate alignment with the

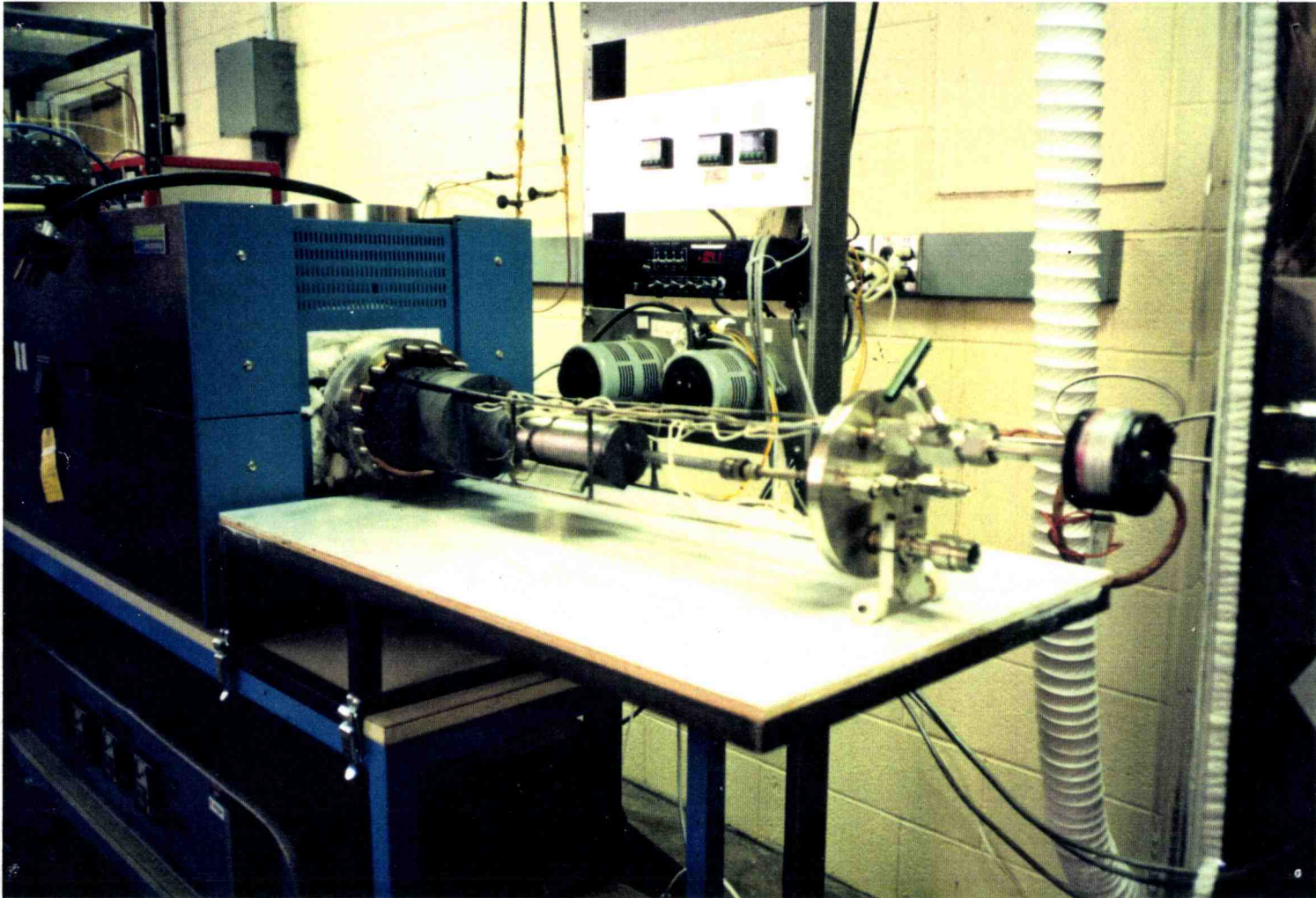


Figure 4.3 Internal Assembly Photograph.

reaction chamber and allow transport through the bellows and sliding gate valve. The skid assembly hangs from the pumped fitting when pulled into the load-lock (deflection of the pushrod as it is inserted creates the need for the skid). The load-lock flange is mounted onto a wheeled carriage that runs on a track for easy access to the substrate holder. The skid assembly and flange carriage are pictured in Figure 4.4.

The substrates are held onto the holder by three lipped graphite pins. The pins are pushed in, the edges holding the substrate tightly in place.

The push rod is permanently attached to the trap to allow easy alignment of the substrate holder with the reaction chamber; consequently, it is imperative that the sliding gate valve separating the load-lock and process tube not be closed when the push rod is through it. A safety interlock was put in so that the valve fails in place on power failure. Administrative control, however, is the only mode of prevention against operator error.

4.3 Precursor Heater Assembly

As calculated in section 3.4, the precursor heater needs to generate approximately 200 watts of resistive heat to create adequate gaseous precursors for deposition. This is not an extraordinary amount of power; however, the resulting power density of 17 W/in² is high, creating an increased

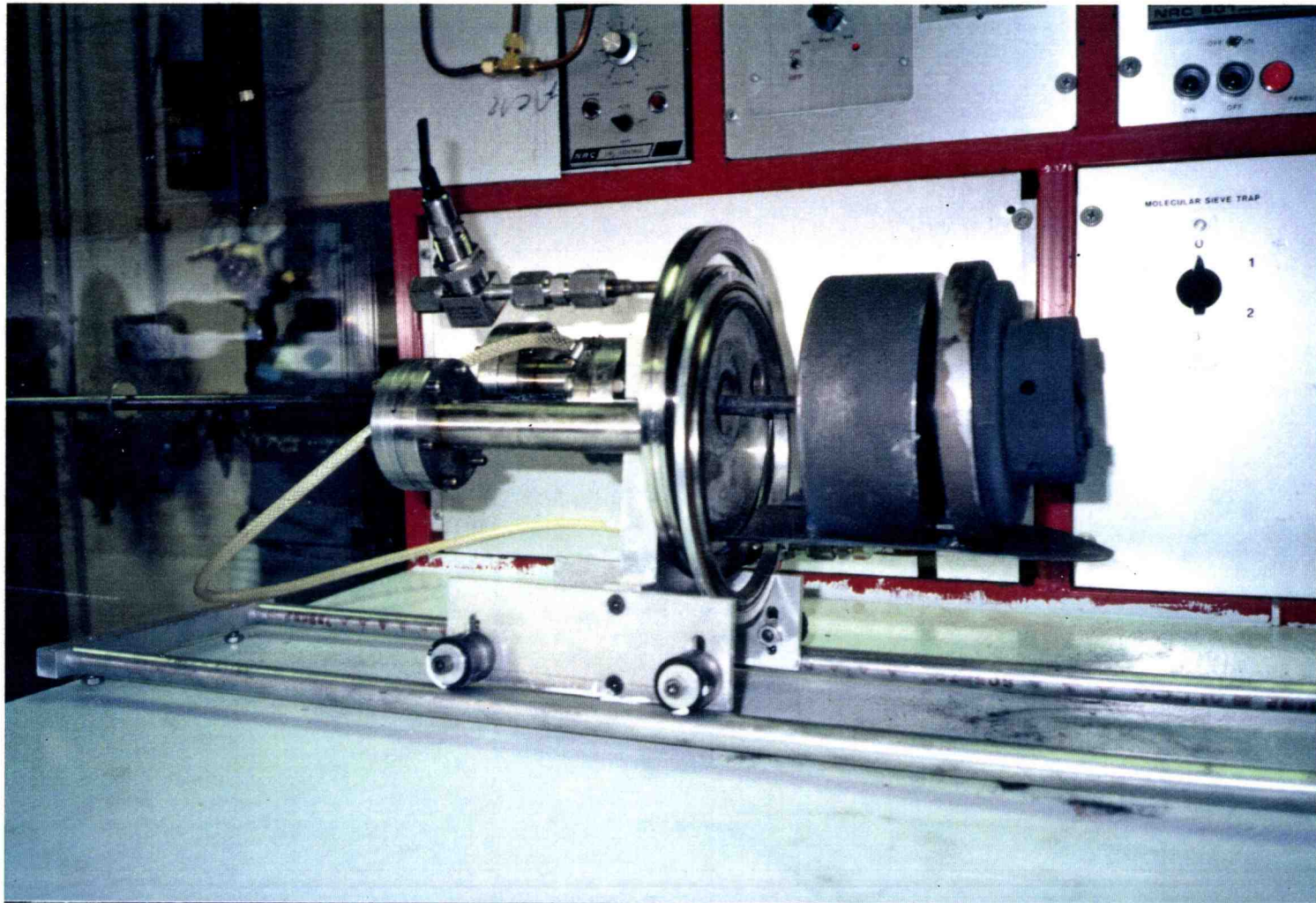


Figure 4.4 Skid Assembly and Flange Carriage Photograph.

likelihood of element burnout. Further, the size of the crucible limits the length of element wire that can be wrapped. The heater design is therefore dictated by the maximum current the element can carry as well as its total resistance.

A nickel-chromium (nichrome) alloy (NiCr 80) was chosen as the element material. To determine what gauge and length of wire was needed, the failure currents for several gauges were determined. This was done by applying an increasing voltage across a measured length of wire until it burned out. This experiment was performed with the wires exposed to air, a significantly different environment than in the heater assembly. These values, however, were thought to be conservative estimates of element performance. The chosen element material, 24 AWG wire, failed at 5.2 amps.

The maximum length of wire that can be wrapped around the 3 inch long, 1 inch diameter crucible with adequate spacing between wraps is about 10 feet. The resistivity of 24 AWG NiCr 80 wire is 1.657 ohms/ft at room temperature, but increases by 6% upon heating to 975°C. Total resistance of a 10 ft element during operation is, therefore, 17.6 ohms. To generate 200 watts of power, a current of 3.4 amps is needed. This is well below the estimated failure current. This heater configuration, then, should be adequate for the designated operation. In actual operation only about 130 watts (2.7 amps) are needed to reach a crucible temperature of

975°C.

Since the crucible is made of electrically conductive graphite, the heating element must be isolated from it to prevent short circuiting. Initial constructions used alumina fish spline beads threaded onto the nichrome wire. These didn't provide adequate heat transfer, however, because of the small amount of contact area between the wire and the inside of the beads (conduction being the prevalent mode of heat transfer). Heaters built according to this design quickly burned out. Another method of construction, using an electrically insulating, thermally conductive cement, was subsequently used. A thin layer of this high temperature cement was first painted onto the outside of the crucible. The element was then wrapped directly onto the crucible and another layer of cement painted over it. The cement provides excellent thermal contact between the element and crucible and also electrically insulates and mechanically supports the wire.

High temperature insulation (zirconia felt) and thermal radiation shields fill the spaces between the crucible and shell and end caps, as diagrammed in Figure 4.5. The opposing metal foils have low emissivities and absorptivities, thus reducing radiative heat loss. The annulus between the concentric foils is maintained by the end caps which attach to the shell and are supported by the inlet and outlet tubing.

Crucible temperature is controlled by a relay output

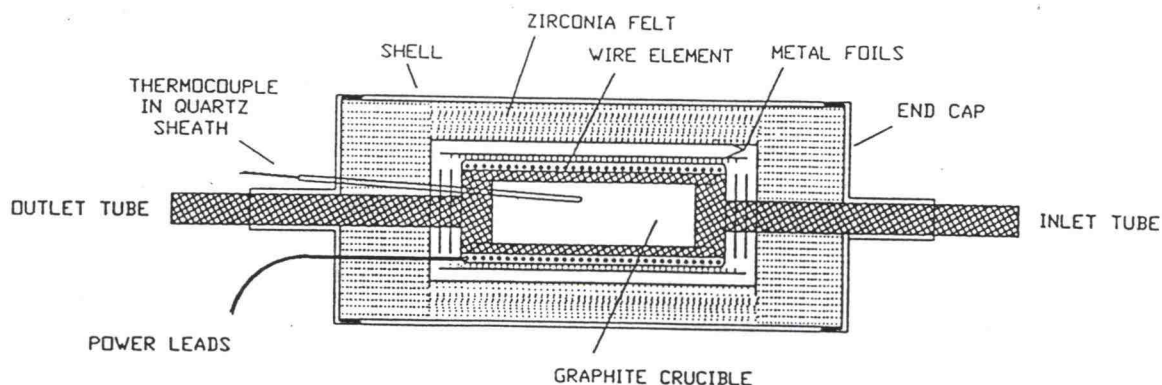


Figure 4.5 Precursor Heater Schematic.

controller. The relay output goes to a voltage regulator where it is adjusted to prevent overcurrent conditions in the element. A quartz-sheathed thermocouple placed inside the crucible provides the temperature input to the controller.

4.4 Ancillary Systems

4.4.1 Heat Removal

To minimize heat transfer from the process tube to external components, copper cooling coils were silver soldered around three inches of each end of the process tube. The solder not only mechanically supports the coils, it enhances heat transfer by increasing the contact area. A closed loop chiller (Neslab HX400) is used to cool water flowing through cooling coils. The chiller bath temperature is maintained at a constant 6°C even at the highest heat loads.

It was discovered that during removal of the substrate

holder the temperatures of the bellows section, process sliding gate valve, and load-lock increased dramatically. There was concern that the temperatures could reach the point that would do damage to the elastomeric o-rings in the sliding gate valve. This should have been expected as the graphite substrate holder is quite nearly a black body and is of significant mass. Consequently, copper cooling coils were added to the bellows section and the load-lock, successfully reducing heat flow to the sliding gate valve.

4.4.2 Compressed Gas Shroud

The HCl used to transport Mn dopant is extremely toxic. Consequently, an exhausted gas cabinet of some sort was desired as a safety precaution against leakage. An assembly was constructed that integrated securing and exhausting of gas cylinders with rack mounting of the mass flow controllers. The close proximity of the cylinders to the mass flow controllers allows short, simple connecting lines. The shroud is comprised of removable, clear plastic panels that affix to an angle iron frame. The shroud encloses the entire assembly, with the feed lines to the inlet flange penetrating through a slit in one panel. Since HCl is denser than air, the shroud is exhausted from the bottom. The exhaust line is tied into nearby hood ductwork. The assembly is on wheels to facilitate connection to the inlet flange.

4.4.3 Substrate Access Hood

In an attempt to maintain a certain degree of cleanliness in an environment that is otherwise ill-suited for quality thin film deposition, an enclosure was built around the load-lock access for changing substrates. This hood is comprised of an angle-iron frame with plexiglass side panels and a removable plastic front access. Filtered compressed air is supplied to the hood to maintain a positive pressure flow out, thus reducing particulates. For the same reason, the inside surfaces of the iron frame are painted, as is the plywood work surface.

Chapter 5 - Operational Results and Design Modifications

5.1 Precursor Heater Performance

Building an internal heater capable of attaining the 900-1000°C temperature necessary for ZnS sublimation proved to be a formidable task. The first heater built failed during heat-up at less than 900°C; the second performed better, holding a temperature of 920°C for a short time. Examination of the failed heaters revealed insufficient attention to detail during construction. In the first, the element short-circuited with a lead wire at a spot that wasn't adequately covered with insulating cement. In the second, the element burned out where the wraps were too close together, creating an area of excessive power density. By improving fabrication methods, subsequent heaters proved to be reliable for sublimation of an entire charge (~20 g) of ZnS (~24 hours).

It was discovered that heaters also failed if cooled too rapidly. Tensile stresses in the contracting element around the still-hot crucible core are enough to break the nichrome wire. Heaters that were cooled slowly worked fine when used again. The cool-down process, however, is long and tedious with the present setup. Consequently, it is easier to build a new heater for each series of depositions.

5.2 Flow Path Modifications

Similar to the development of the internal heaters, the flow assembly also went through a fit-up and refinement process.

ZnS powder (325 mesh) was chosen as the solid precursor material for its large surface area. Deposition rates should increase with surface area. However, the velocity of the carrier gas, 260 m/s at 100 sccm and 0.1 torr, blew the powder into the reactor. ZnS pieces (3-10 mm) were subsequently used with success.

Various mechanical problems also arose. Reinforcements in the support structure were needed to keep tubing connections from coming apart. Also, the substrate holder didn't seat into the end of the reaction chamber very well, allowing process gases to bypass the designated flow path through the substrate holder. This was corrected by chamfering the sharp edges where the substrate holder and the reaction chamber meet.

Design modifications were required to successfully transport the ZnS precursor. After making a series of unsuccessful runs, heavy deposits of sphalerite were found on the inside of the crucible outlet tube. This was believed to be the result of cooling of gaseous precursors by the Ar carrier gas. To alleviate this phenomenon, an Ar preheater, as diagrammed in Figure 5.1, was built. The preheater is

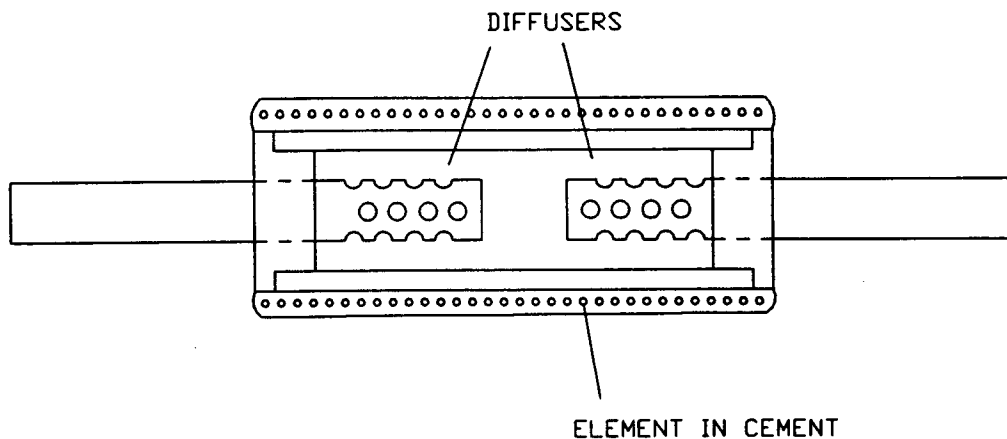


Figure 5.1 Preheater Schematic.

constructed in much the same way as the precursor heaters except that it has diffusers to promote circulation and surface contact and, therefore, heat transfer.

In addition to the preheater, the bore of the crucible outlet tube was increased from $3/16$ inch to $5/16$ inch and the flow path from the crucible to the reaction chamber was straightened in an effort to reduce surface contact and subsequent premature deposition. The Mn heater was removed and the ZnS heater placed in-line with the center tube of the nozzle, through which the Zn and S_2 gas now flowed. The ZnS heater was also placed closer to the reaction chamber. The experimental focus was now on producing quality ZnS films; only after accomplishing this is the addition of dopants

appropriate.

The addition of the Ar preheater virtually eliminated deposition in the tubing; however, concentrated amorphous ZnS spots were now deposited on the substrate. The center tube of the nozzle was made into a diffuser as in the Ar preheater and the flow rate was decreased to about 5 sccm. Spot formation was reduced, but not eliminated. It was later discovered that spot formation resulted largely from the substrate temperature being too low. The transport rate of ZnS at a crucible temperature of 975°C and an Ar flow of 5 sccm is on the order of 1 gram per hour.

5.3 Film Quality

Only after resolving the mechanical and startup issues could a designed experiment begin. Once adequate gaseous precursors are supplied to the reaction chamber, the most important parameter in depositing a ZnS film is the substrate temperature. Here, again, a problem arose. The reaction chamber temperature was measured using a thermocouple penetrating through the inlet end of it. The thermocouple placement was based on the assumption that the reaction chamber temperature was uniform and would therefore be representative of the substrate temperature. At temperature readings of 580°C, however, amorphous ZnS films were formed, indicating the actual substrate temperature was significantly

lower than the reading. Relocation of the thermocouple to the other end of the chamber is hampered by spacial restrictions. Nevertheless, accurate measurement of substrate temperature will require a thermocouple to be placed on or in the holder. This is a complicated issue since the holder is moved between the process and load-lock; a thermocouple must therefore be brought in from the load-lock flange. Optical pyrometry may be another alternative.

Meanwhile, the reactor thermocouple reading was largely ignored and the substrate temperature was regarded as a quantity relative to the controller setpoints of furnace zones 2 and 3 (the substrate is positioned at the interface between the two).

Table 5.1 shows data for films deposited at different nominal temperatures. All other parameters were held constant at the following values: ZnS crucible temperature of 975°C, pressure of 0.06 torr, Ar flow rate of 5 sccm, and process time of 1.5 hours. Thickness measurements were made using

Table 5.1 Deposition Results.

Zone 2,3 setpoint, °C	thickness, μm	index of refraction	Comments
600	-	-	amorphous ZnS spot
625	0.46	-	swirling spectral surface
650	0.64	2.423	even spectral surface
675	0.36	2.335	even spectral surface

step profilometry and ellipsometry; indexes of refraction were measured using ellipsometry.

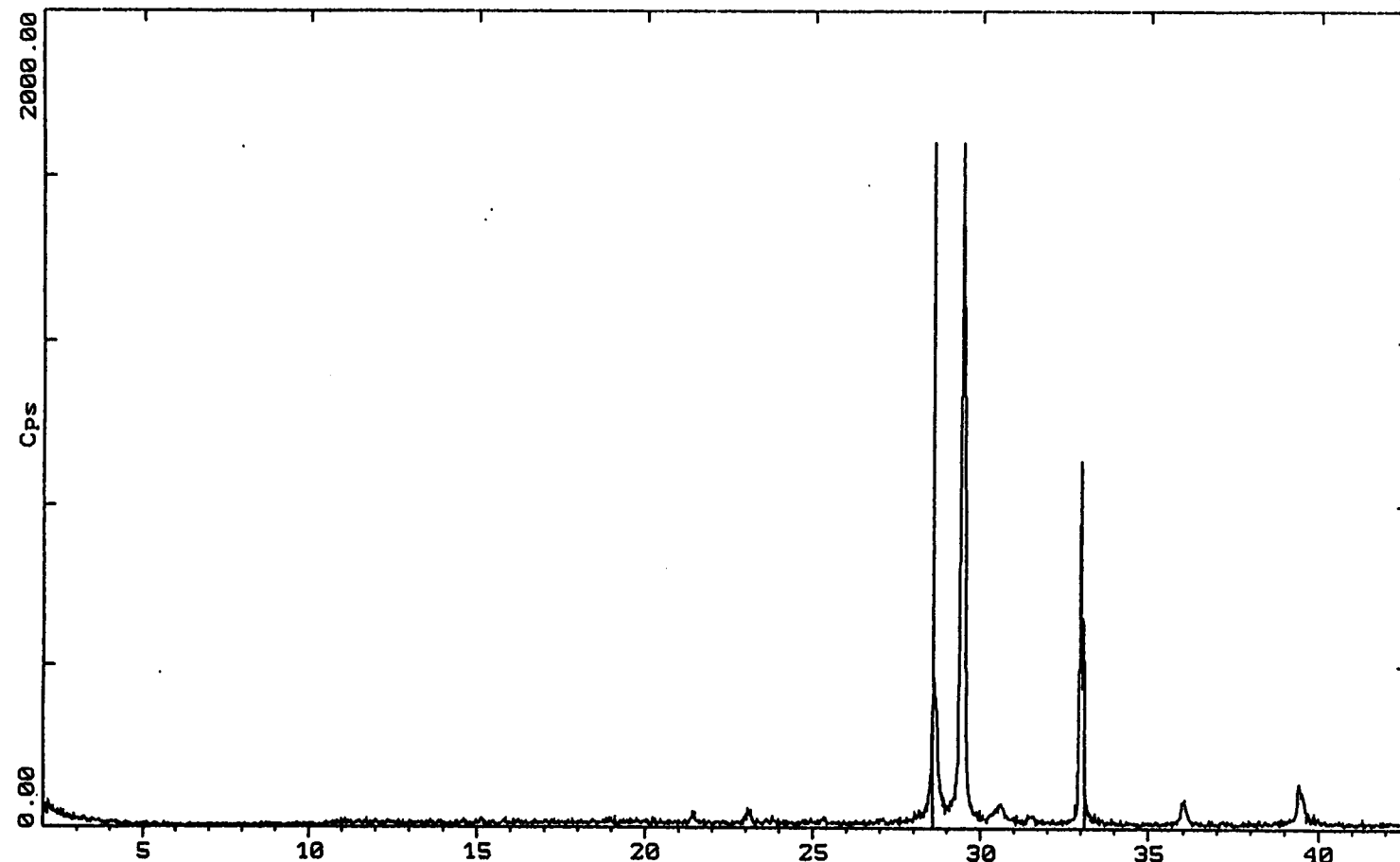
The substrate quality visibly improved with increasing temperature. Further experiments are needed to evaluate deposition characteristics at even higher temperatures. The rate of film deposition varied from 40-70 Å/min, values somewhat lower than those of other CVD systems, but the same as or higher than ALE rates. With the substrate temperature properly controlled, it may be possible to achieve greater deposition rates by increasing the carrier gas flow (assuming the process, at present flows, has not yet reached its kinetic limitation). The indexes of refraction compare favorably to the tabulated value of 2.368, indicating good stoichiometry. Microprobe analysis also indicated a 1:1 Zn:S atomic ratio. Previous depositions at lower temperatures had higher indexes, indicating Zn-rich films.

X-ray diffraction (XRD) analyses show the film reflections to match well with those of crystalline sphalerite. The XRD plot for the film processed with furnace zones 2 and 3 set at 650°C is shown in Figure 5.2. The very large peak ($\theta=29.5^\circ$) is from the silicon substrate.

Figure 5.3 shows a backscattered electron (BSE) micrograph of one of the ZnS films. The crystallite size is estimated to be on the order of 100 nm in equivalent diameter.

2-Theta - Scale

24-Mar-1995 14:52



C:\ND5000\DATA\SC24J003.RAW SC24J003 RTM ZNS 34 (CT: 1.0s, SS:0.020dg, WL: 1.5406Ao, Tim: 5-0566 I ZnS Sphalerite syn (WL: 1.5406Ao)

Figure 5.2 XRD Analysis.

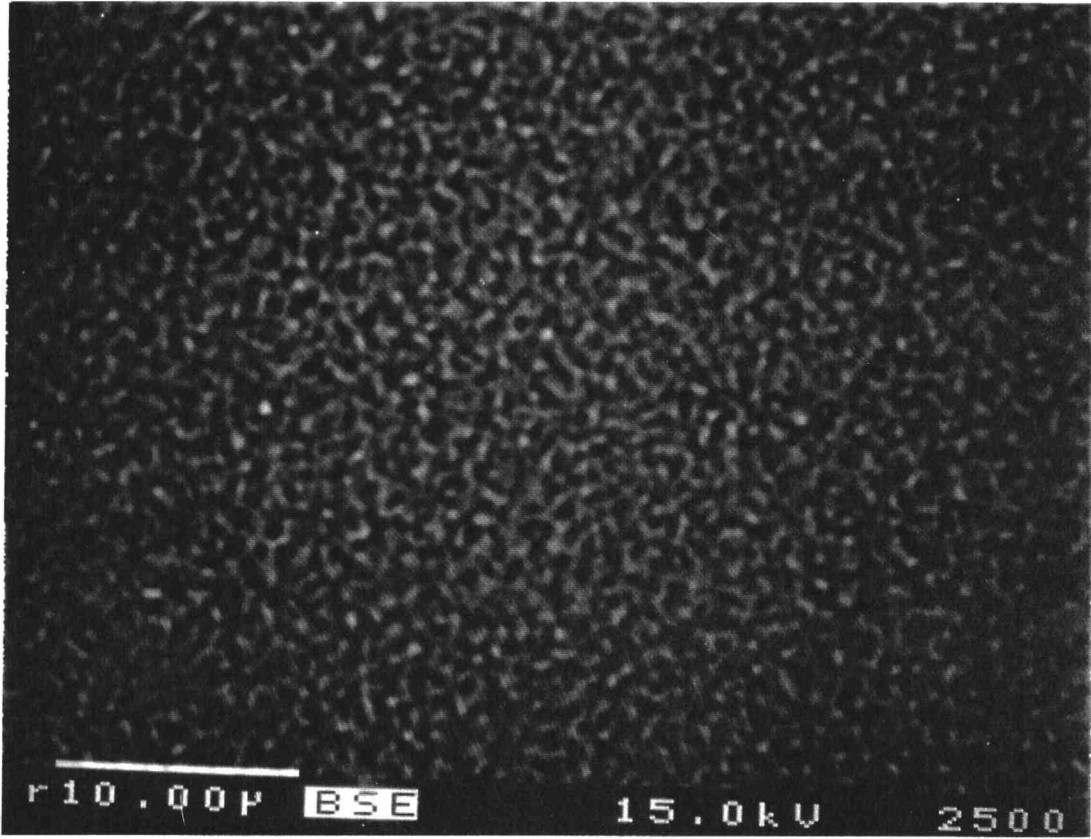


Figure 5.3 BSE Micrograph.

Chapter 6 - Conclusions and Recommendations for Future Work

6.1 Conclusions

A novel, modular experimental HTCVD reactor system was designed and built to deposit ZnS:Mn phosphors and to study the relationships between processing parameters and EL performance.

Preliminary depositions have produced ZnS films of good crystallinity and uniformity. These depositions were performed at very low carrier gas flow rates; even so, deposition rates as fast as those for ALE processes were realized. There is optimism that further investigations may demonstrate much faster rates while maintaining film quality.

A design modification is needed to gain accurate substrate temperature measurements, without which meaningful correlations cannot be made.

Overall, the system appears to be a good vehicle for studying HTCVD processing of ZnS:Mn phosphors.

6.2 Recommendations for Future Work

Before ZnS:Mn deposition experiments can begin in earnest, a couple of system modifications need to be made. First and foremost, a method of gaining accurate substrate temperatures is needed. It is recommended that a thermocouple

be placed inside the graphite substrate holder near the mounting surface. To accommodate the locomotion of the holder, the thermocouple leads can be run through the inside of a tubular push rod. A vacuum-tight feedthrough will be needed at the end of the rod where the external connection is made.

The Mn crucible and heater need to be refitted into the internal assembly. Given the difficulties encountered in transporting the ZnS, it is recommended that the ZnS heater be left where it is and the Mn heater be placed behind it, further from the reaction chamber. Fewer transport problems are expected with Mn since its gaseous precursors are generated at a lower temperature (700°C) than those of ZnS (975°C). It is also recommended, however, that an HCl preheater be incorporated before the Mn heater.

Precursor heater design should be reviewed with the objectives of greater crucible capacity and more reliable operation. With the heaters no longer configured side by side, the crucible diameter can easily be increased (the most effective way of increasing capacity). Different alloys of nichrome (NiCr 70, specifically) and other materials, such as molybdenum, may prove to be better element materials.

Refinements of the skid and internal assemblies can also be made. To obtain quality results, a machinist should be consulted.

Integration of mass spectrometry for analysis of reaction

chamber gases can be done most practicably by routing the probe delivery line through a tubular push rod. This setup, however, requires a long delivery line that subsequently results in long transport times. The likelihood of changing chemistry through gas-phase reactions and deposition losses to the delivery line walls increases with transport time.

The laboratory environment should be upgraded to a standard more amenable to thin film processing. Solutions to improve temperature control and air quality are currently being investigated, and should be followed up on.

Bibliography

1. T. Inoguchi, M. Takeda, Y. Kakihara, Y. Nakata, and M. Yoshida, Digest of 1974 SID International Symposium (1974) 84.
2. W.M. Ang, Oregon State University, M.S. Thesis, 1993.
3. Communicated by Sey-Shing Sun of Planar Systems, Beaverton, Oregon, March 29, 1995.
4. Apple Powerbook product information sheet.
5. Communicated by Sey-Shing Sun of Planar Systems, Beaverton, Oregon, March 27, 1995.
6. A. Mikami, K. Terada, K. Okibayashi, K. Tanaka, M. Yoshida, and S. Nakajima, J. Appl. Phys. 72 (1992) 773.
7. H. Sasakura, H. Kobayashi, S. Tanaka, J. Mita, T. Tanaka, and H. Nakayama, J. Appl. Phys. 52 (1981) 6901.
8. H. Sasakura, H. Kobayashi, S. Tanaka, J. Mita, and T. Tanaka, J. Luminescence 24/25 (1981) 897.
9. H. Ohnishi, K. Yamamoto, and Y. Katayama, Conference Record of the 1985 International Display Research Conference (1985) 159.
10. C. Hsu, Y. Lin, Y. Su, and M. Yokoyama, J. Appl. Phys. 72 (1992) 4655.
11. T. Nire, A. Matsuno, A. Miyakoshi, and K. Ohmi, Jpn. J. Appl. Phys. 33 (1994) 2605.
12. T. Suntola, J. Antson, A. Pakkala, and S. Lindfors, Digest of 1980 SID International Symposium (1980) 108.
13. E. Soininen, "Atomic Layer Epitaxy Color EL Displays", Thin Film Materials Processing Seminar, Oregon State University, September 30, 1994.
14. K. Hirabayashi, H. Kozawaguchi, and B. Tsujiyama, Jpn. J. Appl. Phys. 26 (1987) 1472.
15. J. Yu, K. Jones, P. Holloway, B. Pathangey, E. Bretschneider, T. Anderson, S. Sun, and C. King, J. Electronic Materials 23, no.3 (1994) 299

16. A. Mikami, K. Terada, K. Okibayashi, K. Tanaka, M. Yoshida, and S. Nakajima, *J. Crystal Growth* 110 (1991) 381.
17. A. Mikami, K. Terada, M. Yoshida, and S. Nakajima, *J. Crystal Growth* 117 (1992) 991.
18. Y. Ono, *Acta Polytechnica Scandinavica Ph* 170 (Applied Physics Series No. 170), Fifth International Workshop on Electroluminescence, eds. M. Leskeä and E. Nykänen (Finnish Academy of Technology, Helsinki, 1990) 41.
19. D. Theis, H. Oppolzer, G. Ebbinghaus, and S. Schild, *J. Crystal Growth* 63 (1983) 47
20. T. Shibata, K. Hirabayashi, H. Kozawaguchi, and B. Tsujiyama, *Jpn. J. Appl. Phys.* 26 (1987) L1664
21. J. McKinnis, Oregon State University, M.S. Thesis, 1995
22. Y. Ono, *Electroluminescent Display*, Advanced Research Laboratory, Hitachi, Ltd, Japan, to be published